

Mode-Coupling Theory for Tagged-Particle Motion of Active Brownian Particles

Julian Reichert,¹ Suvendu Mandal,² and Thomas Voigtmann^{1,2}

¹*Institut für Materialphysik im Weltraum, Deutsches Zentrum für Luft- und Raumfahrt (DLR), 51170 Köln, Germany*

²*Department of Physics, Heinrich-Heine Universität Düsseldorf, Universitätsstr. 1, 40225 Düsseldorf, Germany**

(Dated: 2021-07-28)

We derive a mode-coupling theory (MCT) to describe the dynamics of tracer particles in dense systems of active Brownian particles (ABPs) in two spatial dimensions. The ABPs undergo translational and rotational Brownian dynamics, and are equipped with a fixed self-propulsion speed along their orientational vector that describes their active motility. The resulting equations of motion for the tagged-particle density correlation functions describe the various cases of tracer dynamics close to the glass transition: that of a passive colloidal particle in a suspension of ABP, that of a single active particle in a glass-forming passive host suspensions, and that of active tracers in a bath of active particles. Numerical results are presented for these cases assuming hard-sphere interactions among the particles. The qualitative and quantitative accuracy of the theory is tested against event-driven Brownian dynamics (ED-BD) simulations of active and passive hard disks. Simulation and theory are found in quantitative agreement, provided one adjusts the overall density (as known from the passive description of glassy dynamics), and allows for a rescaling of self-propulsion velocities in the active host system. These adjustments account for the fact that ABP-MCT generally overestimates the tendency for kinetic arrest. We also confirm in the simulations a peculiar feature of the transient and stationary dynamical density correlation functions regarding their lack of symmetry under time reversal, demonstrating the non-equilibrium nature of the system and how it manifests itself in the theory.

I. INTRODUCTION

Systems of active Brownian particles (ABPs) are paradigmatic models for non-equilibrium statistical physics [1]. They are a conceptually simple toy model that incorporates both thermalized random Brownian motion, and non-equilibrium active self-propulsion that captures motion typical of biological entities such as cells and micro-organisms, as well as of artificial colloidal microswimmers such as suspended Janus particles driven by an external energy field [2].

While a lot of attention has been devoted to the dilute and moderately dense active fluids, the high-density dynamics of ABP is still less explored. Active particles can form states of collective kinetic arrest, where self-propulsion and steric-hindrance forces balance to form an “active glass” [3, 4]. Active glasses have been identified in computer simulations of ABP [5], as well as in experimental systems employing artificial microswimmer suspensions that are thought to be good realizations of the ABP model [6, 7]. Also computer models of tissue dynamics show glassy states with similar phenomenology [8], and in general, collective dynamics and eventual kinetic arrest by glass formation or jamming of motile entities is considered relevant for our understanding of mechanisms in the crowded interior of organisms (see e.g. Refs. [9–16]).

Theoretical studies of active glasses have so far mostly focused on somewhat simpler model systems, like that of active Ornstein-Uhlenbeck particles (AOUP) [17–21] or

related models [22–25]. The activity in the AOUP system is modeled through non-white noise with a finite persistence time, and in essence this provides for easier theoretical modeling as one does not have to take into account orientational degrees of freedom explicitly. The model is usually also studied without passive Brownian motion, i.e., in the athermal limit. Fewer theoretical studies address the dynamics of thermal ABP at high densities. Arguably, to correctly resolve the orientational degrees of freedom of the ABP becomes important at high densities, where the mean distance between particles is on the order of, or less than the persistence length of self-propulsion.

In the present contribution, we extend our previous approach of using the mode-coupling theory of the glass transition (MCT) to describe the high-density dynamics of ABP in two spatial dimensions [26, 27]. While the previous work focused on the *collective* dynamics of density fluctuations near the active-glass transition, here we complement that theory by equations of motion for the *tagged-particle* dynamical density correlation functions, to study tracer motion near the active- and passive-glass transition. Several points motivate this development: first, the tagged-particle dynamics is the observable that is most often studied in computer simulation of glass-forming systems, because of its better statistics. Second, the tagged-particle correlation functions provide the theoretical basis to derive also equations of motion for the mean-squared displacement (MSD) of tracer particles, which is the convenient observable to extract from experimental studies that investigate active suspensions by direct-imaging techniques [7, 28]. Third, many interesting physical effects arise from the interaction of active with passive particles. This concerns the observation of

* Current address: Physikalisches Institut, Albert-Ludwigs-Universität, 79104 Freiburg, Germany

active tracers moving in a “crowded” environment (previously studied in models with fixed obstacles [29–33]), or the motion of active particles in visco-elastic suspension [34–36]. Also, the embedding of passive probe particles in active fluids provides an interesting case in light of experiments, specifically micro-rheology techniques that assess the dynamics of biological fluids by observation of suspended colloidal particles [37–39]. Such passive tracers have been observed to undergo super-diffusive motion as a clear sign of the non-equilibrium forces active in the bath [40–46]. The effective interactions of passive particles provided by an active bath have also been studied recently in experiment [47].

A further central topic of the present paper is to assess the accuracy of the mode-coupling theory for active Brownian particles (ABP-MCT) in comparison to computer simulation. To this end we employ event-driven Brownian dynamics (ED-BD) computer simulations [5, 48] as a tool to implement the Brownian dynamics of particles with strict hard-sphere no-overlap interactions, and compare the self-intermediate scattering function (SISF) in various setups of active and passive tracer particles in active and passive host systems. This provides a crucial test of the approximations invoked in the theory, and establishes the validity of ABP-MCT for a regime of dense suspensions whose slow structural relaxation is modified by activity. The simulations also allow to test peculiar features of the theoretically predicted correlation functions that relate to the inherent non-equilibrium nature of the model system.

The paper is structured as follows: in Sec. II we recapitulate the ABP-MCT for the collective dynamics, and extend it to include equations of motion for the tagged-particle dynamics of a tracer with possibly different interactions and different activity parameters than the host system. In Sec. III, we demonstrate numerical solutions of the equations of motion for the tracer-correlation functions, and compare the ABP-MCT results to those of our ED-BD simulations: after establishing the baseline in a comparison of passive-in-passive tracer dynamics (Sec. III A), we turn to the motion of an active tracer first in the dilute system (Sec. III B), then in the passive host system (Sec. III C), and finally we discuss the motion of passive and active tracers in the dense active host system (Secs. III D and III E). A small note on the differences between transient and stationary averages in the correlation functions (Sec. III F) follows. Section IV provides concluding remarks.

II. THEORY

A. Mode-Coupling Theory

The ABP-MCT describes tagged-particle motion in ABP as coupled to the dynamics of collective density fluctuations; the corresponding equations for the latter have been derived by Liluashvili et al. [26] and shall be

repeated here for completeness.

We study systems of N ABP in two spatial dimensions, with positions \vec{r}_k and orientation angles φ_k ($k = 1, \dots, N$). The stochastic equations of motion are

$$d\vec{r}_k = \mu \vec{F}_k dt + \sqrt{2D_t} d\vec{W}_k + v_0 \vec{n}(\varphi_k) dt, \quad (1a)$$

$$d\varphi_k = \sqrt{2D_r} dW_{\varphi_k}, \quad (1b)$$

where the \vec{F}_k are the direct interaction forces. The Brownian motion is driven by independent Wiener processes $d\vec{W}_k$ and dW_{φ_k} , where D_t and D_r are the respective diffusion coefficients. The particle mobility μ is chosen to obey the equilibrium detailed-balance condition, $\mu = \beta D_t$, where $\beta = 1/kT$ is the inverse temperature. Active motion is modeled as a fixed self-propulsion of velocity v_0 along the orientation vector of each particle, $\vec{n}(\varphi_k) = \vec{n}_k = (\cos \varphi_k, \sin \varphi_k)^T$. This term is formally treated as an (arbitrarily strong) non-equilibrium perturbation to the passive equilibrium dynamics.

The theory will be applied to particles that experience spherically symmetric direct interactions akin to those of hard spheres. We fix the units of length and time via the particle diameter σ and the translational diffusion time σ^2/D_t . This leaves two fundamental parameters to characterize the ABP motion, viz., the rotational diffusion coefficient D_r and the self-propulsion velocity v_0 .

Translating the equations of motion, Eqs. (1), according to the theory of Markov processes one obtains the (backward) Smoluchowski operator Ω^\dagger that drives the time evolution of observables,

$$\Omega^\dagger = \sum_{k=1}^N D_t (\vec{\nabla}_k + \beta \vec{F}_k) \cdot \vec{\nabla}_k + D_r \partial_{\varphi_k}^2 + v_0 \vec{n}_k \cdot \vec{\nabla}_k. \quad (2)$$

The Smoluchowski operator is the sum of an equilibrium operator and an active driving term, $\Omega^\dagger = \Omega_{\text{eq}}^\dagger + \delta\Omega^\dagger$, with $\delta\Omega^\dagger = v_0 \sum_k \vec{n}_k \cdot \vec{\nabla}_k$. Where convenient, we split off the rotational part of the operator, $\Omega_R^\dagger = D_r \sum_k \partial_{\varphi_k}^2$, denoting the remainder as its translational part, $\Omega_T^\dagger = \Omega^\dagger - \Omega_R^\dagger$. The direct interaction forces are assumed to derive from a potential, $\vec{F}_k = -\vec{\nabla}_k U$, so that $p_{\text{eq}} \propto \exp[-\beta U]$ is the passive-equilibrium solution of the Smoluchowski equation for $v_0 = 0$.

The central quantity of ABP-MCT are the angle-resolved density fluctuations, $\varrho_l(\vec{q}) = \sum_{k=1}^N \exp[i\vec{q} \cdot \vec{r}_k] \exp[i l \varphi_k] / \sqrt{N}$, and the corresponding transient dynamical correlation functions

$$\Phi_{ll'}(\vec{q}, t) = \langle \varrho_l^*(\vec{q}) \exp[\Omega^\dagger t] \varrho_{l'}(\vec{q}) \rangle_{\text{eq}}. \quad (3)$$

Here, angular brackets $\langle \cdot \rangle$ denote the usual *equilibrium* ensemble average, formed with the Boltzmann weight p_{eq} , while the time evolution is understood to contain the full non-equilibrium dynamics. The subscript “eq” is implicit in the following, except in cases where we compare equilibrium and non-equilibrium averages. The transient correlation functions are at the heart of the

integration-through transients (ITT) formalism to derive expressions for non-equilibrium transport coefficients that are of generalized Green-Kubo type. In principle, they are accessible in experiment and simulation when the non-equilibrium perturbation – the particles' activity in our case – is suddenly switched on starting from a passive-equilibrium state.

A Mori-Zwanzig projection operator scheme allows to derive an exact equation of motion of the transient density correlation function, by projecting the dynamics onto the angle-resolved density fluctuations. One gets [26], in matrix notation with respect to the angular-mode indices,

$$\begin{aligned} \partial_t \Phi(\vec{q}, t) + \omega(\vec{q}) \cdot \mathbf{S}^{-1}(q) \cdot \Phi(\vec{q}, t) \\ + \int_0^t dt' \mathbf{m}(\vec{q}, t - t') \cdot (\mathbf{1}\partial_{t'} + \omega_R) \cdot \Phi(\vec{q}, t') = \mathbf{0}, \quad (4) \end{aligned}$$

to be solved with initial condition $\Phi(\vec{q}, 0) = \mathbf{S}(q)$. Here $S_{ll'}(q) = \delta_{ll'} S_l(q)$ is the equilibrium static structure factor of the passive system, assumed to be a known input quantity to the theory. Since we assume the interaction potential between the particles to be spherically symmetric, the only non-trivial term is $S_0(q) \equiv S(q)$, while $S_l(q) = 1$ for all $l \neq 0$. In general, we will assume the system to remain homogeneous and isotropic, so that the positional ($l = l' = 0$) correlation functions depend on the wave vector \vec{q} only through its magnitude $q = |\vec{q}|$.

The matrix $\omega(\vec{q}) = \omega_T(\vec{q}) + \omega_R = -\langle \varrho_l^*(\vec{q}) \Omega^\dagger \varrho_{l'}(\vec{q}) \rangle$ is the (negative) matrix element of the Smoluchowski operator, separated into its contributions to the translational and the rotational degrees of freedom,

$$\omega_{T, ll'}(\vec{q}) = \delta_{ll'} q^2 D_t - \delta_{|l-l'|,1} \frac{iqv_0}{2} e^{-i(l-l')\theta_q} S_l(q), \quad (5a)$$

$$\omega_{R, ll'} = \delta_{ll'} l^2 D_r. \quad (5b)$$

Here, $\vec{q} = q(\cos \theta_q, \sin \theta_q)^T$. The non-trivial properties of the solutions of Eq. (4) for active particles (as compared to the established solutions for passive particles) stem from the fact that $\omega_T(\vec{q})$ is a tri-diagonal matrix and couples different l -modes.

The memory kernel $\mathbf{m}(\vec{q}, t) = \mathbf{M}(\vec{q}, t) \cdot \omega_T^{-1}(\vec{q})$ is the focus of MCT approximations. Assuming that the major contribution to these retarded friction effects on the motion of particles stems from the overlap of fluctuating forces with density-pair modes, MCT sets

$$\begin{aligned} M_{l_1 l_2}(\vec{q}, t) \approx \frac{n}{2} \frac{1}{(2\pi)^2} \int d\vec{k} \sum_{l_3 l_4 l_3' l_4'} \mathcal{V}_{l_1 l_3 l_4}^\dagger(\vec{q}, \vec{k}, \vec{p}) \times \\ \times \Phi_{l_3 l_3'}(\vec{k}, t) \Phi_{l_4 l_4'}(\vec{p}, t) \mathcal{V}_{l_2 l_3' l_4'}(\vec{q}, \vec{k}, \vec{p}) \quad (6) \end{aligned}$$

with $n = N/V$ the density of the system, $\vec{q} = \vec{k} + \vec{p}$, and vertices $\mathcal{V}^\dagger = \mathcal{V} + \delta\mathcal{V}^\dagger$. The vertex \mathcal{V} is the same as in

the passive-equilibrium theory,

$$\mathcal{V}_{l_1 l_3 l_4}(\vec{q}, \vec{k}, \vec{p}) = D_t \delta_{l_1, l_3 + l_4} \left[(\vec{q} \cdot \vec{k}) c_{l_3}(k) + (\vec{q} \cdot \vec{p}) c_{l_4}(p) \right], \quad (7a)$$

while the active contribution enters only \mathcal{V}^\dagger ,

$$\begin{aligned} \delta\mathcal{V}_{l_1 l_3 l_4}^\dagger(\vec{q}, \vec{k}, \vec{p}) = \frac{iv_0}{2} \delta_{|l_1 - l_3 - l_4|, 1} S_{l_1}(q) \times \\ \times \left[k e^{-i(l_1 - l_3 - l_4)\theta_k} S_{l_1 - l_4}(k) (c_{l_1 - l_4}(k) - c_{l_3}(k)) \right. \\ \left. + p e^{-i(l_1 - l_3 - l_4)\theta_p} S_{l_1 - l_3}(p) (c_{l_1 - l_3}(p) - c_{l_4}(p)) \right]. \quad (7b) \end{aligned}$$

In these expressions, $c_l(q)$ is the direct correlation function, related to the static structure factor by $S_l(q) = (1 - n c_l(q))^{-1}$. In particular, $c_l(q) = 0$ for all $l \neq 0$.

B. Mode-Coupling Theory for Tagged-Particle Motion

We now consider a tagged (tracer) particle embedded in the N -particle system described above, with position \vec{r}_s and orientation φ_s . Its equation of motion shall be as Eq. (1), where the three relevant parameters are the diffusion coefficients D_t^s and D_r^s , and the tagged-particle self-propulsion velocity v_0^s . The interaction forces between the tracer and the host-system particles can in principle also differ from the one among the host particles; for example, the tracer could be of different size. For simplicity, we focus here on tracers of equal size and interactions as the host particles, $\sigma^s = \sigma$, and all parameters that are not explicitly given are taken as identical to those of the host system. Note however that we specifically allow for the case of a passive tracer in an active bath, or vice versa, i.e., of specific interest is the case $v_0^s \neq v_0$.

The tagged-particle density fluctuations $\varrho_l^s(\vec{q}) = \exp[i\vec{q} \cdot \vec{r}_s] \exp[i l \varphi_s]$ define the tagged-particle transient density correlation function

$$\phi_{ll'}^s(\vec{q}, t) = \langle \varrho_l^{s*}(\vec{q}) \exp[\Omega^\dagger t] \varrho_{l'}^s(\vec{q}) \rangle, \quad (8)$$

where Ω^\dagger is given by Eq. (2) with the sum over particles extended to include the tagged particle. The positional density-correlation function $\phi_{00}^s(q, t)$ is also referred to as the self-intermediate scattering function (SISF). The derivation of the MCT equations of motion for $\phi^s(\vec{q}, t)$ proceeds in analogy to the derivation for the collective counter-part $\Phi(\vec{q}, t)$:

A Mori-Zwanzig projection onto the tagged-particle density fluctuations, using the projection operator $\mathcal{P} = \sum_l \varrho_l^s(\vec{q}) \langle \varrho_l^{s*}(\vec{q}) \rangle$ together with the Dyson decomposition

$$\begin{aligned} \partial_t \exp[\Omega^\dagger t] = \Omega^\dagger \mathcal{P} \exp[\Omega^\dagger t] + \Omega^\dagger \mathcal{Q} \exp[\Omega^\dagger t] \\ + \Omega^\dagger \mathcal{Q} \int_0^t dt' \exp[\Omega^\dagger \mathcal{Q}(t - t')] \Omega^\dagger \mathcal{P} \exp[\Omega^\dagger t'], \quad (9) \end{aligned}$$

yields an equation of motion for the density-correlation function: inserting Eq. (9) into Eq. (8),

$$\begin{aligned} \partial_t \phi^s(\vec{q}, t) &= -\boldsymbol{\omega}^s(\vec{q}) \cdot \phi^s(\vec{q}, t) \\ &+ \int_0^t dt' \mathbf{K}^s(\vec{q}, t-t') \cdot \phi^s(\vec{q}, t') \end{aligned} \quad (10)$$

where $\boldsymbol{\omega}^s(\vec{q})$ is given by the analog of Eq. (5),

$$\omega_{T, l'}^s(\vec{q}) = \delta_{l'l} q^2 D_t^s - \delta_{|l-l'|, 1} \frac{i q v_0^s}{2} e^{-i(l-l')\theta_q}, \quad (11a)$$

$$\omega_{l'}^s(\vec{q}) = \omega_{T, l'}^s(\vec{q}) + l'^2 D_r^2 \delta_{l'l}. \quad (11b)$$

The Mori-Zwanzig memory kernel is given by

$$K_{l'}^s(\vec{q}, t) = \left\langle \varrho_l^s(\vec{q})^* \Omega^\dagger \mathcal{Q} \exp[\Omega^\dagger \mathcal{Q} t] \Omega^\dagger \varrho_{l'}^s(\vec{q}) \right\rangle. \quad (12)$$

In this expression, the spherical symmetry of the direct particle interactions imposes $\Omega_R^\dagger \varrho_{l'}^s(\vec{q}) \in \text{span}_m \{ \varrho_m^s(\vec{q}) \}$, and together with the fact that Ω_R^\dagger is self-adjoint with respect to the scalar product defined by the equilibrium average, it implies that to both sides of the exponential in Eq. (12), one can replace Ω^\dagger by Ω_T^\dagger .

Equation (10) is treated further in order to rewrite the memory kernel $\mathbf{K}^s(\vec{q}, t)$ into a friction memory kernel: we set $\mathcal{P}' = -\sum_{l'} \varrho_{l'}^s(\vec{q}) (\boldsymbol{\omega}_T^s)_{l'l}^{-1} \langle \varrho_{l'}^{s*}(\vec{q}) \Omega_T^\dagger$ to take out the one-particle reducible dynamics by a further Dyson decomposition,

$$\begin{aligned} \exp[\Omega^\dagger \mathcal{Q} t] &= \exp[\Omega^\dagger \mathcal{Q}' \mathcal{Q} t] \\ &+ \int_0^t dt' \exp[\Omega^\dagger \mathcal{Q}(t-t')] \Omega_T^\dagger \mathcal{P}' \mathcal{Q} \exp[\Omega^\dagger \mathcal{Q}' \mathcal{Q} t']. \end{aligned} \quad (13)$$

Inserting into Eq. (12) results in

$$\mathbf{K}^s(t) = \mathbf{M}^s(t) - \int_0^t dt' \mathbf{K}^s(t-t') \cdot \boldsymbol{\omega}_T^{s,-1} \cdot \mathbf{M}(t') \quad (14)$$

(dropping the \vec{q} dependence for notational convenience). Equations (10) and (14) can be combined to a single equation of motion for the density correlator,

$$\begin{aligned} \partial_t \phi^s(\vec{q}, t) + \boldsymbol{\omega}^s(\vec{q}) \cdot \phi^s(\vec{q}, t) \\ + \int_0^t dt' \mathbf{m}^s(\vec{q}, t-t') \cdot (\mathbf{1} \partial_{t'} + \boldsymbol{\omega}_R^s) \cdot \phi^s(\vec{q}, t') = \mathbf{0}, \end{aligned} \quad (15)$$

where we have set $\mathbf{m}^s(t) = \mathbf{M}^s(t) \cdot \boldsymbol{\omega}_T^{s,-1}$. The exact microscopic expression for the irreducible memory kernel is as in Eq. (12), with the replacement of the projected time-evolution operator by the further reduced one,

$$M_{l'}^s(\vec{q}, t) = \left\langle \varrho_l^s(\vec{q}) \Omega_T^\dagger \mathcal{Q} \exp[\mathcal{Q} \Omega^\dagger \mathcal{Q}' \mathcal{Q} t] \mathcal{Q} \Omega_T^\dagger \varrho_{l'}^s(\vec{q}) \right\rangle. \quad (16)$$

MCT proceeds by approximating this memory kernel in terms of density pair modes. For the description of

tagged-particle motion, the first non-trivial overlap is with the mixed modes $\varrho_{l_3}^s(\vec{k}) \varrho_{l_4}^s(\vec{p})$, so that inserting a projector onto such pairs to both sides of the exponential operator in Eq. (16), and splitting the resulting dynamical four-point correlation function into a product of two-point correlation functions, one obtains

$$\begin{aligned} M_{l_1 l_2}^s(\vec{q}, t) &\approx \frac{n}{(2\pi)^2} \int d\vec{k} \sum_{l_3 l_4} \mathcal{W}_{l_1 l_3 l_4}^s(\vec{q}, \vec{k}) \times \\ &\times \Phi_{l_3, 0}(\vec{k}, t) \phi_{l_4 l_2}^s(\vec{p}, t). \end{aligned} \quad (17)$$

In this expression, we have anticipated that the equilibrium part of the vertex is obtained in analogy to Eq. (7a), but due to the assumption of a tagged particle that is separate from the N host particles, a further symmetry under $\vec{k} \leftrightarrow \vec{p}$ allows to reduce the integral to twice that over the first term in the vertex expression. Making further use of the symmetry of the interaction potential, which ensures that all $c_l(q)$ with $l \neq 0$ vanish, the tagged-particle vertex can be summarized as

$$\begin{aligned} \mathcal{W}_{l_1 l_3 l_4}^s(\vec{q}, \vec{k}) &= (D_t^s c^s(k))^2 \left[\delta_{l_1 l_4} \delta_{l_3 0} (\vec{q} \cdot \vec{k})^2 \right. \\ &+ \delta_{|l_1 - l_3 - l_4|, 1} \frac{i(\vec{q} \cdot \vec{k}) k e^{-i(l_1 - l_3 - l_4)\theta_k}}{2D_t^s} (v_0 S(k) \delta_{l_1 l_4} - v_0^s \delta_{l_3 0}) \left. \right]. \end{aligned} \quad (18)$$

The tagged-particle direct correlation function $c^s(k)$ quantifies the interactions between the tracer particle and the host-system particles. In the simplest case of a structurally identical (but possibly different in activity) tracer, $c^s(k) = c(k)$.

Note that in Eq. (18) *both* the tagged-particle self-propulsion velocity v_0^s , and the host system's v_0 enter. Thus the dynamics of a passive tracer in an active host system is modified both indirectly, through an implicit v_0 -dependence of the correlation function $\Phi_{l, 0}(\vec{k}, t)$ appearing in Eq. (17), and directly through a modified coupling vertex.

In summary, the tagged-particle correlation functions are determined from a MCT memory equation with a memory kernel $\mathbf{M}^s(\vec{q}, t)$ that couples bi-linearly to the collective density correlators $\Phi(\vec{k}, t)$, and the tagged-particle correlators $\phi^s(\vec{p}, t)$. Thus, Eqs. (15)–(18) can be solved once the collective dynamics has been determined.

C. Small-Wavenumber Limit

The SISF is connected to the MSD of the tracer particle in the low- q limit,

$$\phi_{00}^s(q, t) = 1 - \frac{q^2}{4} \delta r^2(t) + \mathcal{O}(q^4), \quad (19)$$

where the factor 4 holds in two spatial dimensions. It is thus instructive to discuss the $q \rightarrow 0$ limit of the MCT

memory kernel $\mathbf{m}^s(\vec{q}, t)$. We include its derivation here for completeness, although a detailed discussion of the MSD and its comparison to experiment is outside the scope of the present contribution and is relegated to separate publications [49, 50].

The derivation is simplified by noting the transformation rule for the correlation functions under a rotation of \vec{q} . Invariance of the equilibrium distribution and the Smoluchowski operator under a rotation of the coordinate system implies $\Phi(\vec{q}', t) = \mathbf{u}^\dagger(\psi) \cdot \Phi(\vec{q}, t) \cdot \mathbf{u}(\psi)$ if \vec{q}' is obtained from rotating \vec{q} by an angle ψ and $u_{l'l'}(\psi) = \delta_{ll'} \exp[i\psi]$ is the unitary representation of the rotation group. The quantities

$$\tilde{\Phi}_{l'l'}(q, t) = e^{i(l-l')\theta_q} \Phi_{l'l'}(\vec{q}, t) \quad (20)$$

are thus functions of the wave vector through $q = |\vec{q}|$ only. We define corresponding isotropized matrices for the other quantities that appear in the equations of motion and denote them by tildes. It is readily checked that the Mori-Zwanzig equations of motion are invariant under this mapping. There further holds $\Phi_{-l, -l'}^s(\vec{q}, t) = (-)^{l-l'} \Phi_{l'l'}^s(\vec{q}, t)$, and it follows that the diagonal elements are isotropic and even functions of q . In particular, $\Phi_{00}(q, t)$ is indeed isotropic and real-valued, in agreement with Eq. (19).

Since $\tilde{\mathbf{m}}^s(q, t) = \tilde{\mathbf{M}}^s(q, t) \cdot \tilde{\omega}_T^{s,-1}(q)$, the discussion of the low- q limit requires an expression for the inverse of $\tilde{\omega}_T^s(q)$. Note that the latter is a symmetric tri-diagonal matrix,

$$\tilde{\omega}_{T, l'l'}^s(q) = \delta_{ll'} D_t^s q^2 - \delta_{|l-l'|, 1} \frac{i q v_0^s}{2}. \quad (21)$$

This simple structure allows to derive a closed form for the matrix elements of its inverse,

$$(\tilde{\omega}_T^s)^{-1}_{l'l'} = \frac{1}{\Delta} \left(\frac{i q v_0^s}{D_t^s q^2 + \Delta} \right)^{|l-l'|} \quad (22)$$

setting $\Delta = \sqrt{(D_t^s q^2)^2 + (v_0^s q)^2}$. This is readily checked by direct computation of $\tilde{\omega}_T^s \cdot \tilde{\omega}_T^{s,-1}$. A direct derivation of this result is given in Appendix A.

It is worth stressing that implicit in this result is the recognition that the Mori-Zwanzig equations based on the angle-resolved density fluctuations are formulated for elements $\phi_{l'l'}^s(\vec{q}, t)$ of an infinite-dimensional matrix algebra spanned by the angular indices. It is customary (and necessary for numerical computation) to introduce some angular-index cutoff L such that $l, l' \in [-L, L]$. However, the operations of introducing such cutoff and of taking the inverse in the limit $q \rightarrow 0$ do not commute for $\tilde{\omega}_T^s(q)$. Numerical evaluation in fact confirms that for $v_0^s \neq 0$, the inversion of the finite-dimensional matrix yields an asymptotic behavior $\sim 1/q^2$ for the (00) element of the inverse for all even cutoff values L , while the same element approaches a constant for all L odd. On the infinite-dimensional algebra, Eq. (22) confirms the asymptote $1/(v_0^s q)$ for $l = l' = 0$ and $v_0^s \neq 0$. Obtaining

this asymptote is crucial in deriving the correct $q \rightarrow 0$ limit of the ABP-MCT equations.

It is also remarkable that the $q \rightarrow 0$ limit of Eq. (22) does not commute with $v_0^s \rightarrow 0$. In physical terms, any small tracer activity is eventually felt at large enough length scales, i.e., if $q \ll q_* = v_0^s/D_t^s$. Expansion of Eq. (22) yields

$$(\tilde{\omega}_T^s)^{-1}_{l'l'} \sim \begin{cases} 1/(D_t^s q^2) \delta_{ll'} & \text{for } v_0^s = 0, \\ \frac{1}{v_0^s q} i^{|l-l'|} \left(1 - |l-l'| \frac{q}{q_*} \right) + \mathcal{O}(q) & \text{for } v_0^s \neq 0. \end{cases} \quad (23)$$

It requires some care to check that the $q \rightarrow 0$ expansion of the memory integral in Eq. (15) remains regular and produces terms of leading order $\mathcal{O}(q^2)$ in the case of the (00) element, as required by Eq. (19). In the equilibrium theory, this is readily noted by realizing that the vertex \mathcal{W}^s , Eq. (18) is of $\mathcal{O}(q^2)$, so that $\tilde{m}_{00}^s(q, t) \sim \mathcal{O}(q^0)$ combines with the $\mathcal{O}(q^2)$ order of $\partial_{t'} \phi_{00}^s(q, t)$. The appearance of non-diagonal terms in both $\tilde{\mathbf{m}}^s(q, t)$ and $\tilde{\phi}^s(q, t)$, and of a potentially “dangerous” term of $\mathcal{O}(q)$ in the vertex \mathcal{W}^s , complicate matters in the ABP-MCT. After checking the different contributions individually, as detailed in Appendix B, one obtains an equation for the MSD,

$$\begin{aligned} \partial_t \delta r^2(t) + \int_0^t dt' \hat{m}_{00}^s(t-t') \partial_{t'} \delta r^2(t') \\ = 4D_t^s - 2iv_0^s \sum_{\pm} \hat{\phi}_{\pm 1, 0}^s(t) \\ + 4 \sum_{\pm} \int_0^t dt' \hat{m}_{0, \pm 1}^s(t-t') (\partial_{t'} + D_r^s) \hat{\phi}_{\pm 1, 0}^s(t'), \end{aligned} \quad (24)$$

where $\hat{m}_{l'l'}(t) = \lim_{q \rightarrow 0} \tilde{m}_{l'l'}(q, t)/q^{|l-l'|}$ for $|l-l'| \leq 1$. Equation (24) reduces to the MCT equation for the MSD of a passive tracer [51, 52] when $v_0^s = 0$, where the non-diagonal elements of the correlators vanish. In the case of an active tracer particle, a further equation determines the off-diagonal low- q correlator, $\hat{\phi}_{\pm 1, 0}^s(t) = \lim_{q \rightarrow 0} \tilde{\phi}_{\pm 1, 0}^s(q, t)/q$,

$$\begin{aligned} (\partial_t + D_r) \hat{\phi}_{\pm 1, 0}^s(t) = \frac{iv_0^s}{2} \\ - 2 \int_0^t dt' \hat{m}_{\pm 1, \pm 1}^s(t-t') (\partial_{t'} + D_r) \hat{\phi}_{\pm 1, 0}^s(t'). \end{aligned} \quad (25)$$

Explicit expressions for the memory kernels appearing in Eqs. (24) and (25) are given in Appendix B.

Equations (24) and (25) determine the MSD of an active or passive tracer in an active or passive bath, once the corresponding tagged-particle correlation functions at finite \vec{q} have been determined and with these the low- q memory kernels $\hat{\mathbf{m}}(t)$. As we discuss elsewhere [49, 50], in the non-interacting case where $\hat{m}_{l'l'}^s(t) \equiv 0$, Eqs. (24) and (25) confirm the well-known analytical expression for the MSD of a free ABP.

D. Numerical Solution of MCT Equations

The ABP-MCT equations were solved numerically with an algorithm outlined in Ref. [26], using a discrete wave-number grid $q_i = (i + 1)\Delta q/2$, $i = 1, \dots, M$ with a grid size of $M = 128$ and step size $\Delta q \simeq 0.3$, implying a large-wave-number cutoff $Q = 40\sigma$. The integrals are performed for \vec{q} placed along the y -axis, and the correlation functions for different wave-vector orientations that are required in the memory-kernel integrals are obtained by their known transformation behavior under spatial rotations [26]. Angular-mode indices were considered with a cutoff $l \in [-L, L]$ with $L = 1$, which is deemed sufficient for the range of self-propulsion velocities that we study within the theory here.

We apply the theory to hard-disk systems, where the only relevant state parameter in equilibrium is the packing fraction, $\varphi = (\pi/4)n\sigma^2$. The equilibrium static structure factor of the 2D hard-disk system was obtained from density-functional theory (DFT) [53]. This differs slightly from the structure factor used in previous studies of two-dimensional hard disks in MCT, where either modified hypernetted-chain (MHNC) has been used [52] or the empirical Baus-Colot formula [26]. No qualitative changes are imposed by these different choices; but the predicted numerical value of the glass-transition density depends both on the choice of $S(k)$ and the parameters of the discretization in the wave-vector integrals.

E. Brownian Dynamics Simulations

To compare the theoretical predictions with simulation results, we performed ED-BD simulations of size-polydisperse hard-disk systems with $N = 1000$ particles (adjusting the box size to achieve the desired packing fraction for any given realization of polydispersity). Particle sizes were drawn randomly from a uniform distribution of width 0.1σ .

The ED-BD algorithm has been described in detail for passive systems [48]. For every Brownian time step of length τ_B , the particles are assigned random Gaussian displacements Δx with a variance that sets the short-time diffusion coefficient. To resolve particle overlaps, the displacements are translated into pseudo-velocities, $v = \Delta x/\tau_B$, and an event-driven molecular-dynamics simulation segment of length τ_B is performed with elastic collisions between the particles. This algorithm reproduces the Smoluchowski dynamics of the passive system if τ_B is chosen not too large [48].

The algorithm is extended ad hoc to active particles by assigning Gaussian displacements to the particles with an individual drift corresponding to the active driving term. For this, also particle orientation angles are tracked and incremented by Gaussian displacements to establish rotational diffusion. A version of this algorithm has first been used by Ni et al. [5] for studying the high-density dynamics of ABP.

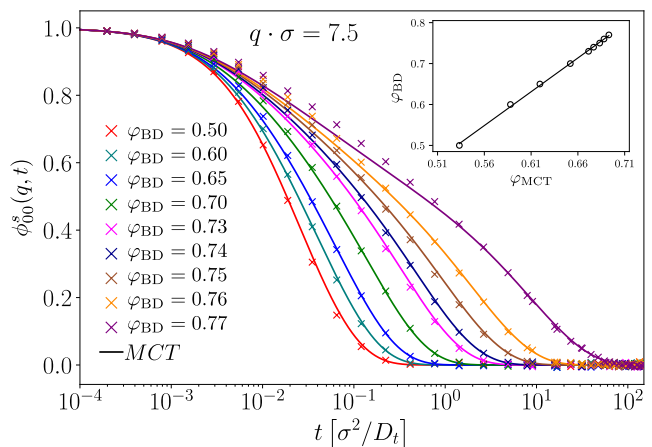


FIG. 1. Tagged-particle density correlation function $\phi_{00}^s(q, t)$ for passive hard-disk systems of packing fraction φ_{BD} as indicated, at wave number $q\sigma = 7.5$. Symbols are results from Brownian dynamics computer simulations, lines are MCT results for packing fractions φ_{MCT} adjusted to give the best description of the data (see inset for the linear relation between φ_{BD} and φ_{MCT}).

For each density we performed at least 200 runs to accumulate statistics for the dynamical correlation functions. The systems were equilibrated first, and then the self-propulsion term was switched on and the systems were brought into stationary state by preparation runs of at least 10^4 Brownian time steps. To study the tracer dynamics, an individual particle was selected within each simulated configuration to closely match the average size of the particles (in order to avoid size-disparity effects that become visible when averaging the motion of tracers of different sizes in the different simulation runs). To improve the statistics, correlation functions were averaged over different starting points in the stationary simulations.

We hence compare in the following the *stationary* correlation functions obtained from the simulation with the *transient* ones obtained by ABP-MCT, under the salient assumption that the two quantities are at least qualitatively similar. For the fully active system, the simulation statistics was also sufficient to calculate the transient dynamical correlation functions, obtained from the simulation-ensemble average over the passive-equilibrium starting configurations. We will for this case discuss the similarities and differences between the two quantities.

III. RESULTS

A. Passive Dynamics

We begin by establishing the level of accuracy that can be expected from MCT by comparing to our simulations of a passive hard-disk system. It is well known that MCT provides a semi-quantitative description of the

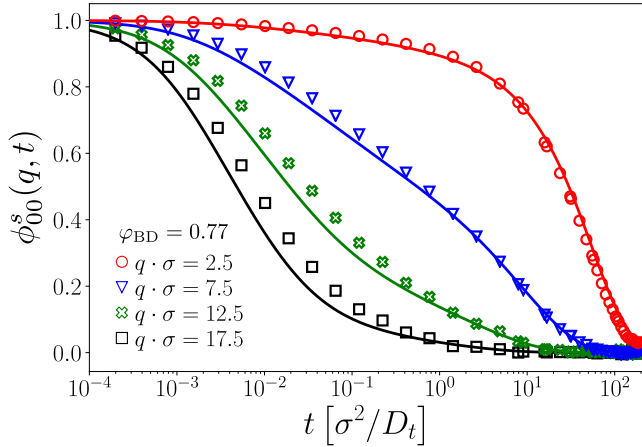


FIG. 2. Tagged-particle density correlation function $\phi_{00}^s(q, t)$ for passive hard-disk systems of packing fraction $\varphi_{\text{BD}} = 0.77$, for different wave numbers as indicated. Symbols are BD simulation results, lines are MCT with effective packing fractions.

relaxation dynamics in a density range just below the glass-transition density, after an adjustment of packing fractions [54] that accounts for errors both in $S(q)$ and those inherent to MCT.

With such an adjustment of the packing fraction, our solutions of the MCT equations for passive hard disks indeed match the computer simulation results very well. Anticipating that the glassy dynamics is driven by fluctuations around the nearest-neighbor peak in the static structure factor, the adjustment of packing fractions is performed by treating φ_{MCT} as a free fit parameter such that at wave number $q\sigma = 7.5$ the long-time structural relaxation matches best that of the simulation at a given packing fraction φ_{BD} . Due to its better sampling statistics, we chose to fit the tagged-particle density correlation function rather than its collective counterpart; at this wave number, no essential change is expected from this [54]. In agreement with earlier studies of similar spirit [52, 54] the thus adjusted MCT gives a quantitative account of the dynamics (Fig. 1). Moreover, a free fit of the obtained φ_{MCT} -vs- φ_{BD} relation for a range of simulations at $\varphi_{\text{BD}} \geq 0.5$, confirms a linear relationship between the two quantities (inset of Fig. 1). Considering that within MCT asymptotically close to the glass transition, a distance parameter that is asymptotically linearly related to the control-parameter distance governs the long-time dynamics, the linear relationship found from the free fit corroborates that the adjustment procedure simply accounts for a well-understood error of MCT in predicting quantitatively the numerical value of the glass-transition point.

Once the mapping of packing fractions is established for the density-fluctuation dynamics of the relevant length scale, MCT also accounts well for the dynamics at other wave numbers in the range covering the relevant variations in $S(q)$ (Fig. 2). The agreement remains very

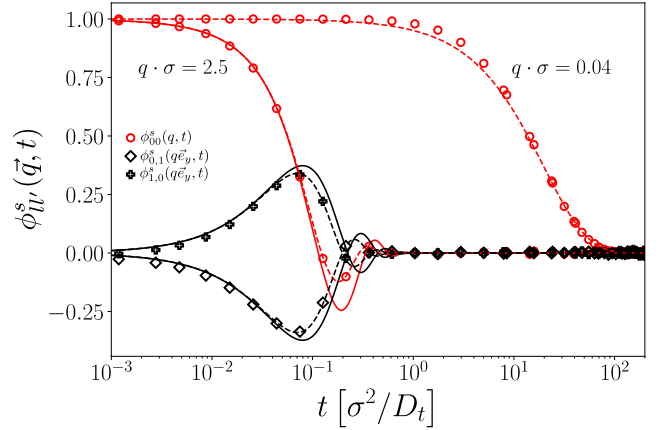


FIG. 3. Correlation functions $\phi_{ll'}^s(\vec{q}, t)$ for a single active Brownian particle with self-propulsion velocity $v_0^s = 8D_t/\sigma$ and rotational diffusion coefficient $D_r^s = 1D_t/\sigma^2$, at a wave vector $\vec{q} \cdot \sigma = 2.5\vec{e}_y$, for $(ll') = (00)$ (circles), $(1, 0)$ (crosses), and $(0, 1)$ (diamonds). Symbols are BD simulation results; solid lines are the solution of the Mori-Zwanzig equations with angular-mode cutoff $L = 1$, dashed lines with $L = 10$. For $\vec{q} \cdot \sigma = 0.04\vec{e}_y$, $\phi_{00}^s(q, t)$ is shown from the simulation (circles) together with the diffusive asymptote (dashed line; see text).

good down to $q\sigma \approx 2.5$ in our simulations, although it is known from similar comparisons in three-dimensional hard-sphere-like systems that for still smaller q , deviations systematically set in [54]. Also as found previously in 3D, the description of the short-time dynamics deteriorates at large q . These effects appear similarly in our 2D comparison and establish the relevant q range over which MCT is expected to quantitatively account for the dynamics.

B. Low-Density Active Dynamics

The Mori-Zwanzig equation is an exact rewriting of the equations of motion, and with our choice of projection onto all $\{\varrho_m(\vec{q})\}_{m \in \mathbb{Z}}$, the memory kernel is at least of $\mathcal{O}(n)$. (The same does not hold if one projects only on the positional density fluctuations $\varrho_0(\vec{q})$.) The low-density solution is therefore given by dropping the memory kernel in Eq. (15) and thus as a matrix exponential,

$$\phi^s(\vec{q}, t) = \exp[-\omega^s(\vec{q})t]. \quad (26)$$

The matrix exponential has to be evaluated numerically with some cutoff on the infinite-dimensional matrices, and exemplary solutions for different cutoff L are compared with simulation results in Fig. 3.

The features of the $(ll') = (00)$ correlation functions of a single ABP have been discussed in detail by Kurzthaler et al. [55, 56]. While passive Brownian motion leads to a decay $\sim \exp(-q^2 D_t^s t)$, the persistence length of self-propulsion sets an intermediate- q regime, where the correlation function decays non-monotonically $\approx \text{sinc}(qv_0^s t)$

(exemplified by the $q\sigma = 2.5$ curve in Fig. 3). For $q \rightarrow 0$, the active motion leads to effective enhanced diffusion, $\sim \exp(-q^2 D_{t,\text{eff}}^s t)$ with $D_{t,\text{eff}}^s = D_t^s(1+Pe)$ and the Péclet number $Pe = (v_0^s)^2/2D_t^s D_r^2$ ($q\sigma = 0.04$ in Fig. 3).

Equation (26) readily provides also the solutions for $(ll') \neq (00)$. For example, the functions for $(ll') = (10)$ and (01) display a clear maximum around $t = 2/(qv_0^s)$ and are, for \vec{q} chosen along \vec{e}_y , positive and negative mirror images of each other (crosses and diamonds in Fig. 3), as can be anticipated by inspecting Eq. (11).

The analytical solution for the $(ll') = (00)$ SISF by Kurtzthaler et al. [56] proceeds by an expansion of the characteristic function of the stochastic process in terms of suitable eigenfunctions of the single-particle Smoluchowski operator, the Mathieu functions (in 2D). The extension to $(ll') \neq (00)$ in this representation is straightforward, and we present the calculation in Appendix C. The two analytical approaches necessarily need to coincide; although the equivalence is somewhat tedious to show [57]. We confirm in Appendix C that the Mathieu function basis indeed diagonalizes the matrix $\omega^s(\vec{q})$. It is nevertheless worth checking the quality of the Mori-Zwanzig solution, Eq. (26), with a finite l -cutoff. For the range of parameters that are of interest here, indeed already a cutoff $L = 1$ gives good qualitative agreement (solid lines in Fig. 3), although larger L would be needed to increase the quantitative description of the oscillatory decay of the correlation function in a q -range that probes the length scales of persistent motion of the ABP. Convergence is slow in this regime: a cutoff of $L = 10$ (dashed lines in Fig. 3) would be required to approximate the exact solutions to within line width in the figure. Our simulation results then coincide quantitatively with the matrix-exponential solution.

C. Active Tracer in a Passive Suspension

A first test of the inclusion of self-propulsion forces in ABP-MCT is provided by the dynamics of a single ABP embedded in a dense host suspension of passive particles. The tracer dynamics decays faster with increasing self-propulsion velocity, v_0^s , of the tracer, although the overall influence of self-propulsion in the dense host suspension is relatively weak (Fig. 4). ABP-MCT somewhat underestimates this effect, but in particular at wave numbers q related to the structure-factor maximum, the theory is in good agreement with the simulation. Deviations become most pronounced for low q and large v_0^s ; the deviations at low q are in fact expected already on the basis of passive MCT [54].

The influence of the tracer-particle activity in a passive host medium is most pronounced at low q . This is highlighted by the q -dependent structural relaxation times $\tau^s(q)$ extracted from the correlation functions, determined here for simplicity as the time where the functions have decayed to the value $1/e$. Overall, ABP-MCT provides a good description of the simulation data (Fig. 5),

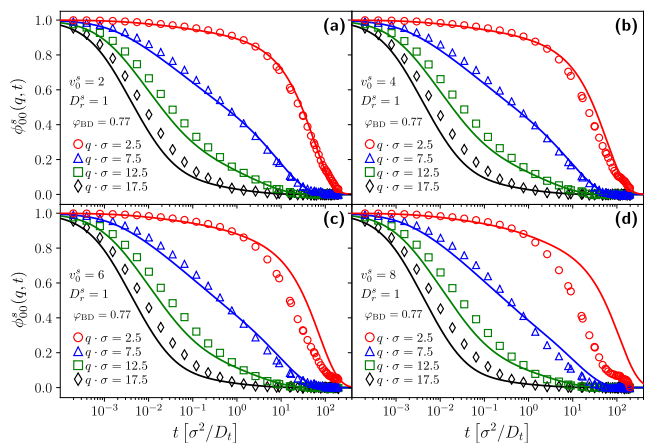


FIG. 4. Self-intermediate scattering function of an active tracer in a passive bath, BD simulations (open symbols) compared with MCT (lines), at different wave numbers as indicated, at fixed packing fraction $\varphi = 0.77$. (a)–(d) exemplify different self-propulsion velocities of the tracer, $v_0^s = 2, 4, 6$, and $8 D_t/\sigma$.

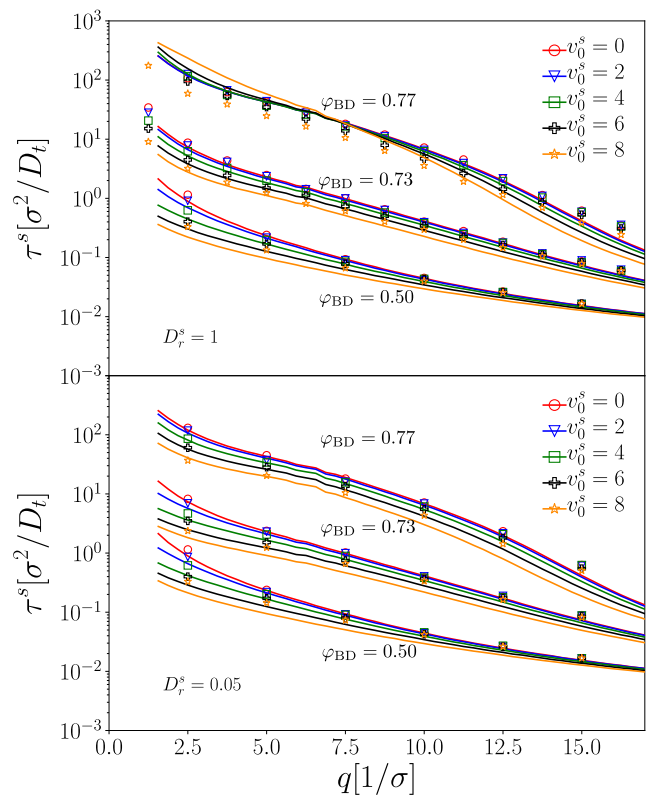


FIG. 5. Structural relaxation time τ^s of the self-intermediate scattering function of an active tracer in a passive host system, for different packing fractions φ as indicated, and as a function of wave number $q\sigma$. Symbols are from ED-BD simulations, lines are from MCT. Top panel: $D_r^s = 1 D_t/\sigma^2$, bottom panel $D_r^s = 0.05 D_t/\sigma^2$.

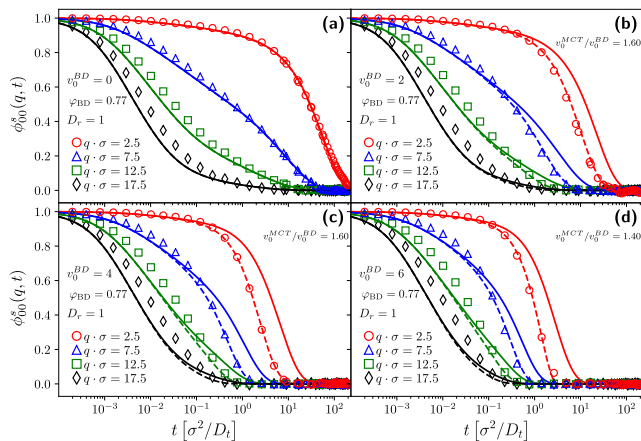


FIG. 6. Self-intermediate scattering function of a passive tracer in an active bath of packing fraction $\varphi = 0.77$. Symbols are BD simulation results, full lines are from MCT; panels (a)–(d) show various wave numbers as indicated for the bath-particle self-propulsion speeds $v_0 = 0, 2, 4$, and $6 D_t/\sigma$. Dashed lines represent MCT with a further empirical mapping of self-propulsion velocities, $v_0^{\text{MCT}} \approx 1.5 v_0^{\text{BD}}$ (as labeled; see text for an explanation).

except for the highest density, $\varphi = 0.77$, studied in the simulations in the case of $D_r^s = 1$. There, the theory predicts a crossing of the τ^s -vs- q curves for different v_0^s of which we find no evidence in the simulations. It has to be kept in mind, that generally, MCT does not accurately account for the relaxation dynamics very close to the glass transition, and the discrepancy observed for the low- q data at $\varphi = 0.77$ may be due to that.

For the parameters investigated here, no qualitative changes are observed between the active-tracer relaxation times and the ones obtained for a passive tracer ($v_0^s = 0$ curves in the figure). For $q \rightarrow 0$, the latter approaches a $1/q^2$ asymptote whose prefactor is related to the long-time diffusion coefficient. The appearance of this diffusive scaling regime is shifted to lower q with increasing tracer activity; the corresponding prefactor decreases and thus indicates a larger long-time diffusion coefficient. This is in qualitative agreement with the overall acceleration of the dynamics due to activity.

Increasing the persistence length of active motion at the same self-propulsion speed and density is predicted by ABP-MCT to cause a stronger enhancement of relaxation; the simulations for $D_r^s = 1$ and $D_r^s = 0.05$ shown in Fig. 5 show this effect for the highest packing fraction and the lower range of v_0^s that we have studied here.

D. Passive Tracer in an Active Suspension

The passive tracer dynamics in a suspension of ABP provides an interesting test case for the application of microrheological techniques in active fluids. Qualitatively, the correlation functions display the same features as

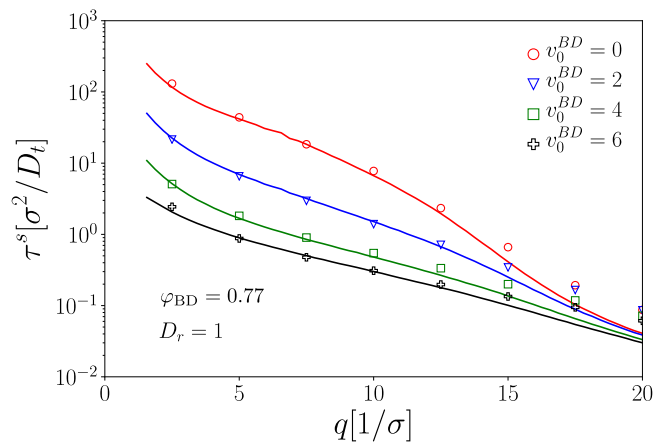


FIG. 7. Wave-number dependent structural relaxation times $\tau^s(q)$ of a passive tracer in an active host system, from ED-BD simulations (symbols) and from MCT (lines), at a fixed packing fraction $\varphi = 0.77$, and various self-propulsion speeds as labeled.

those discussed above for an active tracer in a passive bath (Fig. 6): with increasing activity, the relaxation time shortens, similarly for all wave numbers. The effect of an active bath on a passive tracer is, as perhaps might be expected, much stronger than that of a single active tracer of the same self-propulsion velocity within a passive bath.

Again, MCT is in good qualitative agreement with our BD simulation results. However, MCT underestimates the effect of bath activity on the tracer, i.e., the predicted correlation functions decay too slowly. It is a known effect from other non-equilibrium extensions of MCT, that the theory's approximations tend to underestimate the tendency to fluidization [58, 59]. This is also in line with the general trend of MCT to overestimate the glassiness. Already for sheared colloidal suspensions, an empirical strain scale could be introduced to remedy this effect [60]. Motivated by this finding, we also compare our BD simulations with the MCT predictions where, in addition to the density mapping that is kept fixed throughout after adjusting it for the purely passive system, we also introduce an empirical velocity rescaling. The result (dashed lines in Fig. 6) shows that a roughly parameter-independent mapping of $v_0^{\text{MCT}} \approx 1.5 v_0^{\text{BD}}$ is sufficient to bring MCT in semi-quantitative agreement with simulation.

The relaxation time $\tau^s(q)$ for the case of a passive tracer in the active bath (Fig. 7) demonstrates the much stronger influence of self-propulsion in this case. Here, the strong influence extends over the relevant q -range in structural relaxation, i.e., up to $q\sigma \approx 15$. One also notes that the hydrodynamic limit, where $\tau^s(q) \sim 1/q^2$, is reached only at $q\sigma \lesssim 2$, and there is an intermediate range of wave numbers where a weaker variation of τ^s with q becomes apparent. We shall return to this when discussing the case of an active tracer in an active host

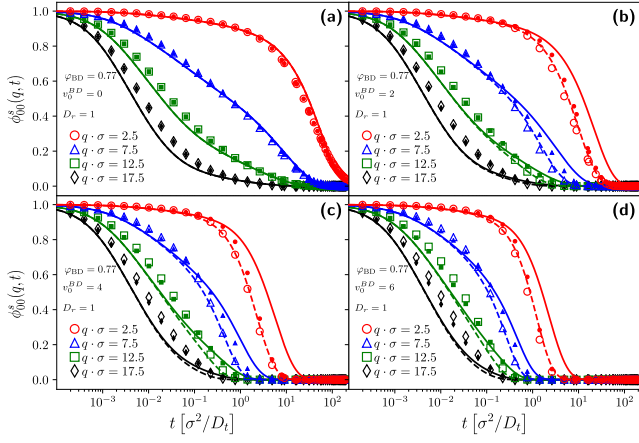


FIG. 8. Self-intermediate scattering functions of an active tracer in an active bath; for fixed bath packing fraction $\varphi = 0.77$ and different self-propulsion velocities $v_0^s = v_0 = 0, 2, 4,$ and $6 D_t/\sigma$ [panels (a)–(d)]. Symbols are results from ED-BD simulations, solid lines are MCT predictions, for various wave numbers as indicated. Dashed lines show the result of MCT with an adjusted self-propulsion velocity $v_0^{\text{MCT}} = 1.5v_0^{\text{BD}}$ (see text). Open symbols indicate simulation averages over the stationary ensemble, while filled symbols represent transient correlation functions defined through the passive-equilibrium average involving the full active dynamics.

system.

E. Active Tracer in an Active Suspension

Finally, the dynamics of an active tracer particle in a fully active system displays qualitatively similar features as the case of a passive tracer in the active bath that we just discussed. The density correlation functions at high densities still decay monotonically, and their relaxation time decreases with increasing v_0 (Fig. 8). As in the previous discussion, MCT qualitatively accounts for this enhanced relaxation, but it underestimates its effect. Again, this can be, for the range of self-propulsion velocities that we consider here, accounted for by a simple empirical adjustment $v_0^{\text{MCT}} = 1.5v_0^{\text{BD}}$, i.e., by assuming again that MCT underestimates the tendency of the nonequilibrium perturbation to fluidize the system.

The evolution of the SISF with host-system packing fraction in general resembles that of the approach to a passive glass transition, at least for the range of self-propulsion speeds that we can compare here with MCT (Fig. 9). The theory provides a reasonable quantitative description of the evolution of the dynamics with packing fraction and self-propulsion velocity close to the glass transition, after performing only two global adjustments: a mapping $\varphi_{\text{BD}} \mapsto \varphi_{\text{MCT}}$ that is fixed in the fully passive system and hence not a specific feature of ABP-MCT, and a mapping $v_0^{\text{BD}} \mapsto v_0^{\text{MCT}}$ that accounts for the stronger effect of activity in simulation compared to

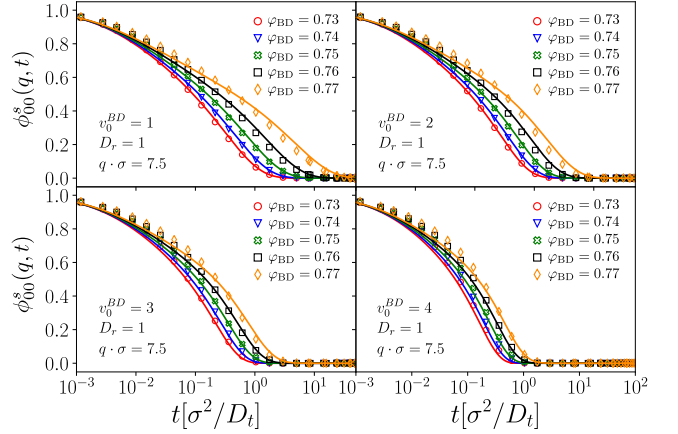


FIG. 9. Self-intermediate scattering functions for an active tracer in an active bath, for self-propulsion velocities $v_0^s = v_0 = 1, 2, 3,$ and $4 D_t/\sigma$ [panels (a)–(d)], at fixed wave number $q\sigma = 7.5$ and for different packing fractions φ as labeled. Symbols are ED-BD simulation results, lines are MCT results with an adjusted self-propulsion velocity (see text).

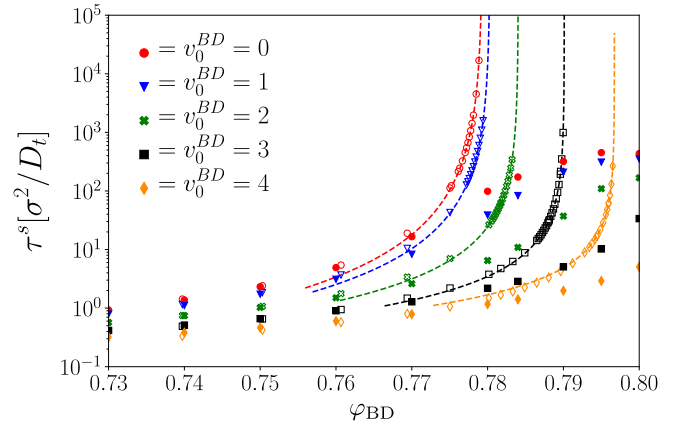


FIG. 10. Structural relaxation time τ^s obtained from the SISF (at wave number $q\sigma = 7.5$) of an active tracer in an active host system, as a function of packing fraction φ , for various self-propulsion velocities $v_0 = 0 \dots 4 D_t/\sigma^2$ as labeled. Filled symbols are results from ED-BD simulation; numerically obtained relaxation times from the solutions of ABP-MCT are shown as open symbols together with corresponding power-law fits (dashed lines).

theory.

In the high-density system, the tagged-particle dynamics of a tracer identical to the bath particles, and the collective dynamics at finite q are strongly coupled, and hence both can be taken as proxies to determine the structural relaxation time. Indeed, we confirm the expected power-law divergence of τ^s within our ABP-MCT results for the tagged-particle dynamics (open symbols and dashed lines in Fig. 10). The ED-BD simulations qualitatively agree in the window of packing fractions $\varphi \lesssim 0.77$, but then deviate strongly from the pre-

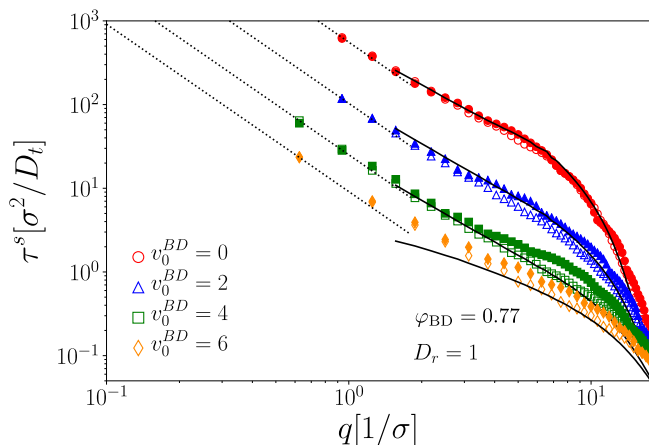


FIG. 11. Wave-number dependence of the structural relaxation time τ^s of an active tracer in an active bath, for packing fraction $\varphi = 0.77$ and different self-propulsion velocities as indicated. ABP-MCT results are shown as solid lines, with $1/q^2$ asymptotes for $q \rightarrow 0$ indicated as dotted lines. ED-BD simulation results are shown as symbols (open: transient; filled: stationary averages). For the ABP-MCT results, $v_0^{\text{MCT}} = 1.5v_0^{\text{BD}}$ has been adjusted.

dicted MCT-like divergence. These deviations become more pronounced with increasing v_0 . Given that the deviations set in while the relaxation times are still moderate, $\tau^s \lesssim 10^2 \sigma^2/D_t$, aging effects from the preparation of the simulation ensemble are unlikely. In fact, MCT is expected to fail close to its predicted glass-transition point due to the appearance of glass-like relaxation processes that the theory neglects [61]. It has been noted previously [5] that these deviations appear to become much stronger in the ABP system, so that the active-glass transition even appears to be shifted up to random-close packing. Note however also that we are dealing with a 2D system, where the appearance of Mermin-Wagner fluctuations cause an additional decay channel for the dynamics as measured by global variables (such as our density correlation functions) [62–64]. A discussion of suitable local variables where the long-range fluctuations specific to the 2D system cancel out, is beyond the scope of the present work.

In the regime where ABP-MCT still describes the structural relaxation times, it also predicts the length-scale dependence of structural relaxation reasonably well. The q -dependence of the relaxation times τ^s follows, in the regime of high densities and self-propulsion velocities covered here, the expected behavior known from passive systems (Fig. 11): as $q \rightarrow 0$, a divergence $\tau^s \sim 1/q^2$ is observed (dotted lines in the figure). There then opens a large intermediate regime, where the behavior is $\tau^s \sim 1/q$; note that from the free-particle dynamics and the inversion of the matrix $\omega^s(\vec{q})$ one indeed expects an $1/v_0^s q$ asymptote to govern the relaxation times [cf. Eq. (23)]. In the ABP-MCT results for the highest activity shown in the figure, the wave-number grid that we

employ in the numerical evaluation of the theory precludes the observation of the $1/q^2$ asymptote in the numerical solutions; it is still seen in the simulations. This is also expected from the structure of the matrix $\omega^s(\vec{q})$: the onset of the diffusive $1/q^2$ asymptote is delayed to larger length scales upon increasing the persistence length of the active motion by increasing v_0 at fixed other parameters.

F. Transient vs. Stationary Averages

In the previous discussion, we have compared simulation results for the SISF that were obtained under stationary averages, i.e., effectively $\phi_{ll'}^{s,\text{stat}}(\vec{q}, t) = \langle \varrho_{ll'}^{s*} \exp[\Omega^\dagger t] \varrho_{ll'}^s(\vec{q}) \rangle_{\text{stat}}$, with the transient quantity $\phi_{ll'}^s(\vec{q}, t)$ defined in Eq. (8), for which ABP-MCT is formulated. This introduced the tacit assumption that the qualitative (and partially quantitative) features of the structural-relaxation dynamics are identical in both quantities. The difference between the two correlation functions is indeed difficult to estimate, since the stationary distribution function of the system is not known.

In the case of an active tracer particle moving in an active host system, discussed in the previous subsection, our simulations allow to address this question numerically. In Fig. 8, both the transient and the stationary SISF are shown (filled and open symbols) for a typical case close to dynamical arrest, i.e., at large packing fraction and various intermediate wave numbers. Both quantities follow each other closely over the parameter regime investigated in that figure. This confirms the approach to compare solutions of ABP-MCT with stationary solutions from simulation or experiment under the premise that the errors inherent in the theory are typically larger than the differences in the different correlation functions. In the ITT-MCT approach to sheared colloidal suspensions, a similar statement holds [65], although there, the transient correlation functions show a regime of faster-than-exponential decay that is absent in the stationary ones. No such qualitative differences are seen in the regime investigated in Fig. 8. Also the structural relaxation times obtained from the two different correlation functions (open and filled symbols in Fig. 11) are qualitatively similar.

In Brownian dynamics that obeys detailed balance, the backward Smoluchowski operator Ω^\dagger driving the time evolution, is self-adjoint in the scalar product weighted with the corresponding equilibrium distribution function: there holds $\langle f^* \Omega_{\text{eq}}^\dagger g \rangle_{\text{eq}} = \langle (\Omega_{\text{eq}}^\dagger f^*) g \rangle_{\text{eq}}$ for arbitrary observables f and g . The active-particle dynamics does not have the property of detailed balance, and hence Ω^\dagger is no longer self-adjoint. For the correlation functions with angular-mode indices l, l' , this amounts to a breaking of symmetry: under the equilibrium dynamics, there holds $\Phi(\vec{q}, t) \stackrel{\text{eq}}{=} \Phi^T(\vec{q}, t)$, while this property is *a priori* lost in the non-equilibrium dynamics. In fact, this is already borne out by the analytical low-density solution (cf. Fig. 3).

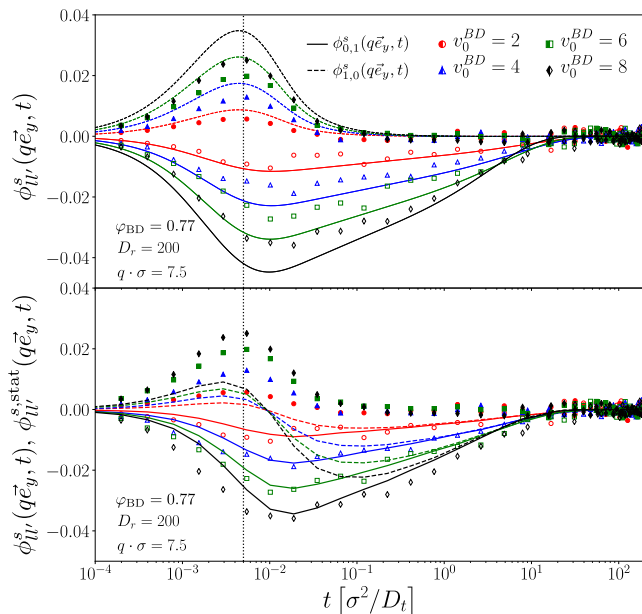


FIG. 12. Stationary and transient tagged-particle correlation functions $\phi_{l,l'}^s(\vec{q}, t)$ of the dense ABP system (active tracer in active host system; packing fraction $\varphi = 0.77$) with $D_r = 200 D_t/\sigma^2$, for $\vec{q}\sigma = 7.5\vec{e}_y$ and self-propulsion velocities $v_0 = 2, 4, 6$, and $8 D_t/\sigma$ as indicated. Top panel: transient correlation functions from ED-BD simulations. Open symbols show $(l, l') = (0, 1)$, filled symbols $(l, l') = (1, 0)$. Solid and dashed lines are the corresponding ABP-MCT results. Bottom panel: comparison of transient (symbols) and stationary (lines) correlation functions both from ED-BD simulations. Here, open/filled symbols are transient correlators for $(l, l') = (0, 1)$ and $(l, l') = (1, 0)$ (as above), and solid/dashed lines the corresponding stationary ones. A vertical dotted line indicates the time scale $1/D_r$.

In ABP-MCT, the resulting asymmetry extends in a peculiar way to the long-time limits of the correlations functions in the ideal glass, the (tagged-particle) non-ergodicity parameters $f_{ll'}^{(s)}$: the feature of the ABP model that rotations always remain ergodic, causes the $(l0)$ matrix elements of the correlation functions to decay on a time scale $1/D_r$ for $l \neq 0$, while only the $(0l')$ matrix elements pick up slow structural relaxation on time scales $t \gg 1/D_r$ and potentially show nonergodic arrest. Technically, this arises due to the presence of the $\omega_R^{(s)}$ contribution in the memory integral in Eqs. (4) and (15); taking the Laplace transform of these equations, one verifies that the zero-eigenmodes of $\omega_R^{(s)}$ always decay exponentially at long times [26]. Intuitively, this expresses that the current configuration of orientational $l \neq 0$ fluctuations are not correlated to how the positional $l' = 0$ fluctuations have evolved (for example, $f_{10}^{(s)} = 0$), while inversely, the current positional $l = 0$ fluctuations are influenced by the distant past evolution of the $l' \neq 0$ orientations through the active driving term ($f_{01}^{(s)} \neq 0$). This still is a subtle prediction, because it hinges on the peculiar structure of

the evolution equations of ABP-MCT, and on the definition of the correlation function. (Recall that in the theory of stochastic processes, it is customary to consider correlation functions that in any stationary process are symmetric [66].)

We check this asymmetry in our ED-BD simulations (Fig. 12). To emphasize the difference, we choose $D_r = 200 D_t/\sigma^2$ such that the time scale $1/D_r$ is much shorter than the structural relaxation time of the system. Indeed, we observe a notable asymmetry in the decay pattern of $\phi_{1,0}^s(\vec{q}, t)$ and $\phi_{0,1}^s(\vec{q}, t)$ in the transient correlation functions (top panel of Fig. 12). The ABP-MCT results are in very good qualitative agreement regarding this asymmetry. Note that here we have chosen $\vec{q} \parallel \vec{e}_y$ such that both correlation functions are real-valued and hence would be identical in equilibrium dynamics. There are thus two remarkable features visible in the plot: first, as predicted by ABP-MCT, the correlation function for $(l, l') = (1, 0)$ decays on the time scale $1/D_r$, where it induces an incomplete relaxation in the $(l, l') = (0, 1)$ correlator. The latter in turn remains non-zero and shows indications of structural relaxation, only decaying on the time scale τ^s (around 1 to $10 \sigma^2/D_t$ for the state points considered here). It is plausible to presume that for higher packing fraction, the quantity $\phi_{0,1}^s(\vec{q}, t)$ will (in the simulationally unattainable ideal case) show structural arrest and thus a finite long-time limit, while $\phi_{1,0}^s(\vec{q}, t)$ clearly decays to zero. Second, the two correlation functions display opposite signs; a feature already encoded in the short-time dynamics of the ABP.

Within the simulation, we also check whether the asymmetry still holds for the stationary correlation functions (lines in the lower panel of Fig. 12). Interestingly, a strong asymmetry remains on time scales small compared to $1/D_r$, while for large times, $t \gg 1/D_r$, the two *stationary* correlation functions approach each other and show structural relaxation that is identical. Thus, extending *bona fide* the ABP-MCT scenario, we conjecture that in the ideal-arrest case, the *stationary* non-ergodicity parameters will all be non-vanishing and form a symmetric matrix, $f_{ll'}^{(s),stat} = f_{l'l}^{(s),stat} \neq 0$, by a non-trivial coupling of orientational and translational fluctuations through the stationary distribution function.

IV. CONCLUSION

We have derived equations of motion for the angle-resolved tagged-particle density correlation functions of tracers in dense systems of active Brownian particles, in the context of the mode-coupling theory of the glass transition and the integration-through transients framework. The numerical solutions of this ABP-MCT theory have been compared to computer simulations of hard-disk ABP for the different cases of active and passive tracers in active and passive host systems. Overall, we have found theory and simulation to be in good qualitative agreement, for a range of densities close to the

glass transition, and for a range of self-propulsion speeds that is not too large. The theory, as known for the passive MCT, overestimates the slowness of structural relaxation, and hence the comparison to simulation data best proceeds with an empirical mapping of densities, and an empirical mapping of self-propulsion speeds in the case of an active host system. After such mapping, the agreement between theory and simulation is near-quantitative.

An interesting feature in the angle-resolved correlation functions is that they are in general non-symmetric matrices of the angular-mode indices. This reflects the non-equilibrium nature of the dynamics, and has first been noted in the ABP-MCT for the collective density fluctuations. We have confirmed this asymmetry directly in our Brownian dynamics (BD) simulations. The simulations point out an interesting difference in the transient correlation functions targeted by the ITT-MCT, and the stationary correlation functions more commonly accessed in experiment and simulation: while both remain asymmetric, there appears to be a time scale after which the time-evolution crosses over to a symmetric form of correlations (as perhaps more intuitively expected). The time scale is associated with the rotational persistence of the ABP; it is thus expected to also play an important role in determining, for example, signatures of persistent motion in other quantities such as the MSD (where superdiffusive regimes indicate the time windows of persistent swimming). Such investigation will be discussed elsewhere.

ACKNOWLEDGMENTS

We acknowledge funding from Deutsche Forschungsgemeinschaft (DFG), as part of the Special Priority Programme SPP 1726 ‘‘Microswimmers’’ (project Vo 1270/7).

Appendix A: Inversion of Frequency Matrix

A tridiagonal $n \times n$ matrix with elements a_{ij} such that $a_{ij} = 0$ whenever $|i - j| > 1$, can be inverted by employing a recursion formula for the elements α_{ij} of the inverse matrix. Setting $a_{ii} = b_i$, $a_{i,i+1} = c_i$, and $a_{i,i-1} = c_i$, Usmani [67] derives

$$\alpha_{ij} = \begin{cases} (-)^{i+j} c_i c_{i+1} \cdots c_{j-1} \theta_{i-1} \phi_{j+1} / \theta_n, & i < j, \\ \theta_{i-1} \phi_{i+1} / \theta_n, & i = j, \\ (-)^{i+j} a_{j+1} a_{j+2} \cdots a_i \theta_{j-1} \phi_{i+1} / \theta_n, & i > j, \end{cases} \quad (\text{A1})$$

where the sequences θ_i and ϕ_i are given by recursion relations,

$$\theta_i = b_i \theta_{i-1} - a_i c_{i-1} \theta_{i-2}, \quad (\text{A2a})$$

$$\phi_i = b_i \phi_{i+1} - c_i a_{i+1} \phi_{i+2}, \quad (\text{A2b})$$

with $\theta_0 = \phi_{n+1} = 1$ and $\theta_{-1} = \phi_{n+2} = 0$.

We apply this result for the $n \times n$ matrix ω_T^s given by Eq. (21) with cutoff L , setting $n = 2L+1$, $i = l+L+1$ and $j = l' + L + 1$ with $l, l' \in [-L, L]$. Identifying then $b_i = D_t^s q^2$, $a_i = c_i = -i v_0^s q / 2$, the recursion relations can be solved in closed form: setting $\Delta = \sqrt{(D_t^s q^2)^2 + (v_0^s q)^2}$, and $\beta_{\pm} = D_t^s q^2 \pm \Delta$, one obtains

$$\theta_i / \theta_n = \frac{2^{n-i} (\beta_+^{1+i} - \beta_-^{1+i})}{\beta_+^{1+n} - \beta_-^{1+n}}, \quad (\text{A3a})$$

$$\phi_i = \frac{(-)^{i+1-n}}{\Delta} 2^{i-2-n} (v_0^s q)^{2(n-i)} \times \left(\beta_+^{i-n} ((v_0^s q)^2 + 2D_t^s q^2 \beta_-) - \beta_-^{i-n} ((v_0^s q)^2 + 2D_t^s q^2 \beta_+) \right) \quad (\text{A3b})$$

From this, the limit $L \rightarrow \infty$ at fixed l, l' and fixed q can be performed. Using $\lim_{L \rightarrow \infty} (\beta_- / \beta_+)^L = 0$, one finally gets Eq. (22).

Appendix B: Low- q Expansion of the Memory Kernel

The limit $q \rightarrow 0$ in the vertex, Eq. (18) is obtained noting $k = p - (\vec{q} \cdot \vec{p}) / p + \mathcal{O}(q^2/p)$ and $k \exp[\pm i \theta_k] = q \exp[\pm i \theta_q] - p \exp[\pm i \theta_p]$ for vectors $\vec{q} = \vec{k} + \vec{p}$. Note that the equilibrium contribution is already of $\mathcal{O}(q^2)$, so that in this case $\tilde{\mathbf{m}}^s(q, t) = \mathcal{O}(q^0)$, and hence the (00) element of Eq. (15) is $\mathcal{O}(q^2)$ in leading order, compatible with the expression Eq. (19).

This is less obvious for the case $v_0^s \neq 0$ or $v_0 \neq 0$. In particular, the low- q expansion of Eq. (18) contains terms of $\mathcal{O}(q)$. One needs to check that these potentially dangerous terms do not contribute in the Mori-Zwanzig equation. Inserting the small- q expansion of $\mathcal{W}^s(\vec{q}, \vec{k})$ into Eq. (17) and performing the integration over the angle θ_k in $\int d\vec{k} = \int k dk d\theta_k$, one obtains

$$\begin{aligned} \tilde{M}_{l'l'}^s(q, t) \sim & \frac{n D_t^{s2}}{8\pi} \int dp \tilde{\phi}_{m'l'}^s(p, t) \times \\ & \left\{ q^2 p^3 (\delta_{l-l',-2} + \delta_{l-l',2} + 2\delta_{l'}) c^s(p)^2 \Phi_{00}(p, t) \delta_{lm'} \right. \\ & + \frac{i q p^3}{D_t^s} (\delta_{l-l',-1} + \delta_{l-l',1}) \tilde{w}_{l,mm'}(p) \tilde{\Phi}_{m0}(p, t) \\ & - \frac{i q^2}{D_t^s} \delta_{l'l'} \partial_p \left(p^3 \tilde{w}_{l,mm'}(p) \tilde{\Phi}_{m0}(p, t) \right) \\ & \left. - \frac{i q^2 p^2}{D_t^s} (\delta_{l-l',-2} + \delta_{l-l',2}) \partial_p \left(p \tilde{w}_{l,mm'}(p) \tilde{\Phi}_{m0}(p, t) \right) \right\} \quad (\text{B1}) \end{aligned}$$

where we have defined

$$\tilde{w}_{l,mm'}(p) = (\delta_{|l-m'|,1} \delta_{m0} v_0^s - \delta_{lm'} \delta_{|m|,1} v_0 S(p)) c^s(p)^2. \quad (\text{B2})$$

For the passive tracer, $v_0^s = 0$, the term $\tilde{w}_{l,mm'}(p)$ is proportional to $\delta_{lm'}$, so that all terms appearing in the

memory kernel, Eq. (B1), couple to $\tilde{\phi}_{l'}^s(p, t)$. But since for this case, the matrix $\tilde{\omega}_T^s(q)$ remains diagonal, the Mori-Zwanzig equations that determine the off-diagonal elements of the correlation-function matrix decouple and, since $\tilde{\phi}_{l'}^s(q, 0) = \delta_{l'}$, these off-diagonal elements all identically vanish. The only contribution to $\tilde{m}_{l'}^s(q, t)$ is thus from the diagonal elements, all of $\mathcal{O}(q^2)$ in leading order. One obtains the only memory kernel that enters the MSD equation, Eq. (24), for the passive tracer:

$$\hat{m}_{00}^s(t) = \frac{nD_t^s}{4\pi} \int dp \tilde{\phi}_{00}^s(p, t) \left\{ p^3 c^s(p)^2 \tilde{\Phi}_{00}(p, t) + \frac{i}{2D_t^s} \delta_{|m|,1} \partial_p p^3 v_0 S(p) c^s(p)^2 \tilde{\Phi}_{m0}(p, t) \right\}. \quad (\text{B3})$$

The first term is the known contribution from passive MCT [52].

In the case of an active tracer particle, Eq. (B1) is simplified by noting a further symmetry of the correlation functions: inverting the coordinate system around the x -axis, $\{x_k, y_k, \varphi_k\} \mapsto \{x_k, -y_k, -\varphi_k\}$, invariance of both the equilibrium distribution and the Smoluchowski operator implies that $\tilde{\Phi}_{l,l'}(q, t) = \tilde{\Phi}_{-l,-l'}(q, t)$. One further checks that $\tilde{\phi}_{l_0}^s(q, t) = \mathcal{O}((iqv_0^s)^{|l|})$ from checking explicitly the terms $(\Omega^\dagger)^n \exp[i\vec{q} \cdot \vec{r}_s]$ stemming from the expansion of $\exp[\Omega^\dagger t]$, and observing that the non-vanishing angular integrals in $\tilde{\phi}_{l_0}^s(q, t)$ require at least the l -fold application of $\delta\Omega^\dagger$.

The low- q expansion of the memory kernel, Eq. (B1), then needs to be combined with the low- q expansion of $\tilde{\omega}_T^{s,-1}(q)$, Eq. (23), in order to check the leading contributions for the different angular indices. The memory kernels that are relevant for the MSD then read

$$\hat{m}_{00}^s(t) = \frac{nD_t^s}{8\pi} \frac{1}{v_0^s} \int dp \tilde{\phi}_{m'l'}^s(p, t) \times \left\{ \delta_{|l'|,1} p^3 \tilde{w}_{0,mm'}(p) \tilde{\Phi}_{m0}(p, t) \right\} \quad (\text{B4})$$

and, determining the coupling to the off-diagonal correlator $\hat{\phi}_{\pm 1,0}^s(t)$,

$$\hat{m}_{0,\pm 1}^s(t) = \frac{nD_t^s}{4\pi} \frac{1}{v_0^s} \int dp \tilde{\phi}_{m'l'}^s(p, t) \times \left\{ iD_t^s p^3 c^s(p)^2 \tilde{\Phi}_{00}(p, t) \delta_{m'0} \delta_{l'0} - \frac{1}{2} \partial_p p^3 \tilde{w}_{0,mm'}(p) \tilde{\Phi}_{m0}(p, t) \delta_{l'0} - \frac{D_t^s}{v_0^s} i \delta_{|l'|,1} p^3 \tilde{w}_{0,mm'}(p) \tilde{\Phi}_{m0}(p, t) \right\}. \quad (\text{B5})$$

with a memory kernel

$$\hat{m}_{\pm 1,\pm 1}^s(t) = \frac{nD_t^s}{8\pi} \frac{1}{v_0^s} \int dp \delta_{|1-l'|,1} \tilde{\phi}_{m'l'}^s(p, t) \times p^3 \tilde{w}_{1,mm'}(p) \tilde{\Phi}_{m0}(p, t). \quad (\text{B6})$$

Appendix C: Mathieu Function Representation

As discussed by Kurzthaler et al. [55, 56], the density-correlation function $\phi_{l'}(\vec{q}, t)$ of a free ABP can be related to the differential equation familiar from the solution of the Schrödinger equation with a periodic potential: One writes, generalizing Ref. [56] to $(l') \neq (00)$,

$$\begin{aligned} \phi_{l'}(\vec{q}, t) &= \int d\varphi d\varphi_0 d\vec{r} d\vec{r}_0 e^{il'\varphi} e^{-il'\varphi_0} e^{i\vec{q} \cdot (\vec{r} - \vec{r}_0)} p(\vec{r}, \varphi, t | \vec{r}_0, \varphi_0) \\ &= \int d\varphi d\varphi_0 e^{il'\varphi} e^{-il'\varphi_0} \tilde{p}(\vec{q}, \varphi, t | \varphi_0), \end{aligned} \quad (\text{C1})$$

where we have used that due to translational symmetry the initial position \vec{r}_0 can be integrated out. The characteristic function \tilde{p} obeys

$$\partial_t \tilde{p} = [-D_t q^2 + iv_0 \vec{n}(\varphi) \cdot \vec{q} + D_r \partial_\varphi^2] \tilde{p}, \quad (\text{C2})$$

where it will be convenient to choose $\vec{q} \parallel \vec{e}_x$. This differential equation is separable, and the angular part reduces (in two spatial dimensions) to the Mathieu equation

$$\left[\frac{d^2}{dx^2} - 2k \cos(2x) \right] f(x) = \lambda(k) f(x), \quad (\text{C3})$$

after substitution $x = \varphi/2$ and $2k = -iv_0 q/D_r$. The solutions of Eq. (C3) are the even and odd Mathieu functions $\text{ce}_{2n}(k, x)$ and $\text{se}_{2n+1}(k, x)$ with eigenvalues $\lambda(k) = a_{2n}(k)$ and $b_{2n+1}(k)$, respectively [68]. They each form an orthonormal basis and can be expressed through their cosine and sine series,

$$\text{ce}_{2n}(k, x) = \sum_{m=0}^{\infty} A_{2m}^{2n}(k) \cos(2mx), \quad (\text{C4a})$$

$$\text{se}_{2n+1}(k, x) = \sum_{m=0}^{\infty} B_{2m}^{2n+1}(k) \sin(2(m+1)x), \quad (\text{C4b})$$

with orthogonality relations for the expansion coefficients

$$\sum_n A_{2m}^{2n} A_{2m'}^{2n} = \delta_{mm'} - \frac{1}{2} \delta_{m0} \delta_{m'0}, \quad (\text{C5a})$$

$$\sum_n B_{2m}^{2n+1} B_{2m'}^{2n+1} = \delta_{mm'}. \quad (\text{C5b})$$

Inserting Eqs. (C4) in Eq. (C2), one can express $\phi_{l'}(\vec{q}, t)$ in Eq. (C1) through its series expansion. For this, we make use of

$$\int_0^{2\pi} \frac{d\varphi}{2\pi} \text{ce}_{2n}(k, \varphi/2) e^{\pm il\varphi} = \frac{1}{2} \left(A_{|2l|}^{2n} + A_0^{2n} \delta_{l0} \right), \quad (\text{C6})$$

$$\int_0^{2\pi} \frac{d\varphi}{2\pi} \text{se}_{2n+1}(k, \varphi/2) e^{\pm il\varphi} = \pm \frac{i \text{sgn } l}{2} B_{|2l|-2}^{2n+1}. \quad (\text{C7})$$

We obtain

$$\begin{aligned} \phi_{ll'}(q\vec{e}_x, t) = e^{-q^2 D t} \sum_{n=0}^{\infty} \left\{ \right. \\ \frac{1}{2} \left(A_{|2l'|}^{2n} + A_0^{2n} \delta_{l'0} \right) \left(A_{|2l|}^{2n} + A_0^{2n} \delta_{l0} \right) e^{-D_r a_{2n}(k)t/4} \\ \left. - \frac{i}{2} (\text{sgn } l)(\text{sgn } l') B_{|2l'|}^{2n+1} B_{|2l|}^{2n+1} e^{-D_r b_{2n}(k)t/4} \right\}. \quad (\text{C8}) \end{aligned}$$

In the special case of the SISF, $l = l' = 0$, only the even expansion terms proportional to $[A_0^{2n}(k)]^2$ remain. Our expression then coincides with Eq. (20) of the Supplementary Material of Ref. [56].

Equation (C8) can be readily rewritten as $\phi_{ll'}(q\vec{e}_x, t) = \sum_n \mathcal{T}_n \exp[-\mathcal{D}_{nn} t] \mathcal{U}_{nl'}$, identifying $\mathcal{U} = \mathcal{T}^{-1}$ with the help of the orthogonality relations Eq. (C5) (see Ref. [57]), and identifying the diagonal matrix

$$\mathcal{D}_{ll} = \begin{cases} D_t q^2 + D_r a_{2n}(k)/4 & \text{for } |l| = 2n, \\ D_t q^2 + D_r b_{2n+1}(k)/4 & \text{for } |l| = 2n + 1. \end{cases} \quad (\text{C9})$$

Thus, $\phi(q\vec{e}_x, t) = \mathcal{T} \cdot \exp[-\mathcal{D}t] \cdot \mathcal{T}^{-1} = \exp[-\omega t]$ where $\omega = \mathcal{T} \cdot \mathcal{D} \cdot \mathcal{T}^{-1}$. It remains to be shown that ω indeed coincides with the Mori-Zwanzig expression, Eq. (11).

To do so, we use the following relations between the expansion coefficients A_{2m}^{2n} and B_{2m}^{2n+1} , and the eigenvalues

$a_{2n}(k)$ and $b_{2n+1}(k)$ that follow from inserting the expansion Eq. (C4) into the Mathieu differential equation (C3),

$$a_{2n} A_{2m}^{2n} = m^2 A_{2m}^{2n} + k(1 + \delta_{m,1}) A_{2m-2}^{2n} + k A_{2m+2}^{2n}, \quad (\text{C10a})$$

$$b_{2n+1} B_{2m}^{2n+1} = (m+1)^2 B_{2m}^{2n+1} + k B_{2m-2}^{2n+1} + k B_{2m+2}^{2n+1}, \quad (\text{C10b})$$

with the convention that $A_{2m}^{2n} = B_{2m}^{2n+1} = 0$ for $m < 0$. Then, a straightforward calculation reveals that indeed

$$\sum_{l''=-\infty}^{\infty} \mathcal{T}_{ll''} \mathcal{D}_{l''l''} \mathcal{T}_{l''l'}^{-1} = (D_t q^2 + D_r l^2) \delta_{ll'} - \frac{i v_0 q}{2} \delta_{|l-l'|,1}, \quad (\text{C11})$$

which confirms the equivalence between the Mathieu-function expansion of Ref. [56] and the present Mori-Zwanzig projection, i.e., between the series expansion Eq. (C8) and the matrix exponential Eq. (26). Both representations remain challenging numerically; the authors of Ref. [56] used a cutoff of $N = 40$ in the series equivalent to Eq. (C8), evaluating the recurrence relation eq. (C10a) with a cutoff of 100. Likewise, as shown in the main text, direct evaluation of the matrix exponential requires matrices of size $(2L+1) \times (2L+1)$ with $L \simeq 10$ in order to achieve similar accuracy.

-
- [1] C. Bechinger, R. Di Leonardo, H. Löwen, C. Reichhardt, G. Volpe, and G. Volpe, *Rev. Mod. Phys.* **88**, 045006 (2016).
- [2] J. R. Howse, R. A. L. Jones, A. J. Ryan, T. Gough, R. Vafabakhsh, and R. Golestanian, *Phys. Rev. Lett.* **99**, 048102 (2007).
- [3] L. M. C. Janssen, *J. Phys.: Condens. Matter* **31**, 503002 (2019).
- [4] L. Berthier, E. Flenner, and G. Szamel, *J. Chem. Phys.* **150**, 200901 (2019).
- [5] R. Ni, M. A. C. Stuart, and M. Dijkstra, *Nature Commun.* **4**, 2704 (2013).
- [6] N. Klongvessa, F. Ginot, C. Ybert, C. Cottin-Bizonne, and M. Leocmach, *Phys. Rev. Lett.* **123**, 248004 (2019); *Phys. Rev. E* **100**, 062603 (2019).
- [7] C. Lozano, J. R. Gomez-Solano, and C. Bechinger, *Nature Materials* **18**, 1118 (2019).
- [8] D. Bi, X. Yang, M. C. Marchetti, and M. L. Manning, *Phys. Rev. X* **6**, 021011 (2016).
- [9] F. Höfling and T. Franosch, *Rep. Prog. Phys.* **76**, 046602 (2013).
- [10] E. H. Zhou, X. Trepát, C. Y. Park, G. Lenormand, M. N. Oliver, S. M. Mijailovich, C. Hardin, D. A. Weitz, J. P. Butler, and J. J. Fredberg, *Proc. Natl. Acad. Sci. USA* **106**, 10632 (2009).
- [11] T. E. Angelini, E. Hannezo, X. Trepát, M. Marquez, J. J. Fredberg, and D. A. Weitz, *Proc. Natl. Acad. Sci. USA* **108**, 4714 (2011).
- [12] B. R. Parry, I. V. Surovtsev, M. T. Cabeen, C. S. O'Hern, E. R. Dufresne, and C. Jacobs-Wagner, *Cell* **156**, 183 (2014).
- [13] J.-A. Park, J. H. Kim, D. Bi, J. A. Mitchel, N. T. Qazvini, K. Tantisira, C. Y. Park, M. McGill, S.-H. Kim, B. Gweon, J. Notbohm, R. S. Jr, S. Burger, S. H. Randall, A. T. Kho, D. T. Tambe, C. Hardin, S. A. Shore, E. Israel, D. A. Weitz, D. J. Tschumperlin, E. P. Henske, S. T. Weiss, M. L. Manning, J. P. Butler, J. M. Drazen, and J. J. Fredberg, *Nature Materials* **14**, 1040 (2015).
- [14] S. Garcia, E. Hannezo, J. Elgeti, J.-F. Joanny, P. Silberzahn, and N. S. Gov, *Proc. Natl. Acad. Sci. USA* **112**, 15314 (2015).
- [15] L. Oswald, S. Grosser, D. M. Smith, and J. A. Käs, *J. Phys. D* **50**, 483001 (2017).
- [16] A. Palamidessi, C. Malinverno, E. Frittoli, S. Corallino, E. Barbieri, S. Sigismund, G. V. Beznoussenko, E. Martini, M. Garre, I. Ferrara, C. Tripodo, F. Ascione, E. A. Cavalcanti-Adam, Q. Li, P. P. Di Fiore, D. Parazzoli, F. Giavazzi, R. Cerbino, and G. Scita, *Nature Materials* **18**, 1252 (2019).
- [17] G. Szamel, E. Flenner, and L. Berthier, *Phys. Rev. E* **91**, 062304 (2015).
- [18] G. Szamel, *Phys. Rev. E* **93**, 012603 (2016).
- [19] E. Flenner, G. Szamel, and L. Berthier, *Soft Matter* **12**, 7136 (2016).
- [20] L. Berthier, E. Flenner, and G. Szamel, *New J. Phys.* **19**, 125006 (2018).
- [21] M. Feng and Z. Hou, *Soft Matter* **13**, 4464 (2017).
- [22] L. Berthier, *Phys. Rev. Lett.* **112**, 220602 (2014).
- [23] D. Levis and L. Berthier, *EPL* **111**, 60006 (2015).
- [24] R. Mandal, P. J. Bhuyan, M. Rao, and C. Dasgupta, *Soft*

- Matter **12**, 6268 (2016).
- [25] R. Mandal and P. Sollich, Phys. Rev. Lett. **125**, 218001 (2020).
- [26] A. Liluashvili, J. Ónody, and Th. Voigtmann, Phys. Rev. E **96**, 062608 (2017).
- [27] A. Liluashvili and Th. Voigtmann, in *NIC Symposium 2018*, John von Neumann Institute for Computing Series, Vol. 49, edited by K. Binder, M. Müller, and A. Trautmann (Forschungszentrum Jülich, Germany, 2018) pp. 313–320.
- [28] J. R. Gomez-Solano, S. Samin, C. Lozano, P. Ruedas-Batuecas, R. van Roij, and C. Bechinger, Sci. Rep. **7**, 14891 (2017).
- [29] A. Morin, N. Desreumax, J.-B. Caussin, and D. Bartolo, Nature Phys. **13**, 63 (2016).
- [30] A. Morin, D. Lopes Cardozo, V. Chikkadi, and D. Bartolo, Phys. Rev. E **96**, 042611 (2017).
- [31] M. Zeitz, K. Wolff, and H. Stark, Eur. Phys. J. E **40**, 23 (2017).
- [32] O. Chepizhko and T. Franosch, Soft Matter **15**, 452 (2019).
- [33] M. Brun-Cosme-Bruny, E. Bertin, B. Coasne, P. Peyla, and S. Rafai, J. Chem. Phys. **150**, 104901 (2019).
- [34] J. R. Gomez-Solano, A. Blokhuis, and C. Bechinger, Phys. Rev. Lett. **116**, 138301 (2016).
- [35] N. Narinder, C. Bechinger, and J. R. Gomez-Solano, Phys. Rev. Lett. **121**, 078003 (2018).
- [36] N. Narinder, C. Bechinger, and J. R. Gomez-Solano, New J. Phys. **21**, 093058 (2019).
- [37] D. Wirtz, Annu. Rev. Biophys. **38**, 301 (2009).
- [38] P. Bursac, G. Lenormand, B. Fabry, M. Oliver, D. A. Weitz, V. Viasnoff, J. P. Butler, and J. J. Fredberg, Nature Materials **4**, 557 (2005).
- [39] K. Nishizawa, K. Fujiwara, M. Ikenaga, N. Nakajo, M. Yanagisawa, and D. Mizuno, Sci. Rep. **7**, 15143 (2017).
- [40] X.-L. Wu and A. Libchaber, Phys. Rev. Lett. **84**, 3017 (2000).
- [41] A. Caspi, R. Granek, and M. Elbaum, Phys. Rev. Lett. **85**, 5655 (2000).
- [42] D. T. N. Chen, A. W. C. Lau, L. A. Hough, M. F. Islam, M. Goulian, T. C. Lubensky, and A. G. Yodh, Phys. Rev. Lett. **99**, 148302 (2007).
- [43] C. Wilhelm, Phys. Rev. Lett. **101**, 028101 (2008).
- [44] N. Gal and D. Weihs, Phys. Rev. E **81**, 020903(R) (2010).
- [45] C. Valeriani, M. Li, J. Novosel, J. Arlt, and D. Marenduzzo, Soft Matter **7**, 5228 (2011).
- [46] A. Lagarde, N. Dagès, T. Nemoto, V. Démery, D. Bartolo, and T. Gibaud, Soft Matter **16**, 7503 (2020).
- [47] E. F. Semeraro, J. M. Devos, and T. Narayanan, J. Chem. Phys. **148**, 204905 (2018).
- [48] A. Scala, Th. Voigtmann, and C. De Michele, J. Chem. Phys. **126**, 134109 (2007).
- [49] J. Reichert and Th. Voigtmann, arXiv:2010.13769 (2021).
- [50] J. Reichert, L. F. Granz, and Th. Voigtmann, Eur. Phys. J. E **44**, 27 (2021).
- [51] M. Fuchs, W. Götze, and M. R. Mayr, Phys. Rev. E **58**, 3384 (1998).
- [52] M. Bayer, J. M. Brader, F. Ebert, M. Fuchs, E. Lange, G. Maret, R. Schilling, M. Sperl, and J. P. Wittmer, Phys. Rev. E **76**, 011508 (2007).
- [53] A. L. Thorneywork, S. K. Schnyder, D. G. A. L. Aarts, J. Horbach, R. Roth, and R. P. A. Dullens, Mol. Phys. **116**, 3245 (2018).
- [54] F. Weysser, A. M. Puertas, M. Fuchs, and T. Voigtmann, Phys. Rev. E **82**, 011504 (2010).
- [55] C. Kurzthaler, S. Leitmann, and T. Franosch, Sci. Rep. **6**, 36702 (2016).
- [56] C. Kurzthaler, C. Devailly, J. Arlt, T. Franosch, W. C. K. Poon, V. A. Martinez, and A. T. Brown, Phys. Rev. Lett. **121**, 078001 (2018).
- [57] J. Reichert, *Transport Coefficients of dense Active Brownian Particles*, Ph.D. thesis, Heinrich-Heine-Universität Düsseldorf (2020).
- [58] O. Henrich, F. Weysser, M. E. Cates, and M. Fuchs, Philos. Trans. R. Soc. London A **367**, 5033 (2009).
- [59] I. Gazuz, A. M. Puertas, T. Voigtmann, and M. Fuchs, Phys. Rev. Lett. **102**, 248302 (2009).
- [60] M. Fuchs, Adv. Polym. Sci. **236**, 55 (2010).
- [61] S. Mandal, T. Franosch, and Th. Voigtmann, Soft Matter **14**, 9153 (2018).
- [62] B. Illing, S. Fritschi, H. Kaiser, C. L. Klix, G. Maret, and P. Keim, Proc. Natl. Acad. Sci. USA **114**, 1856 (2017).
- [63] S. Vivek, C. P. Kelleher, P. M. Chaikin, and E. R. Weeks, Proc. Natl. Acad. Sci. USA **114**, 1850 (2017).
- [64] H. Shiba, Y. Yamada, T. Kawasaki, and K. Kim, Phys. Rev. Lett. **117**, 245701 (2017).
- [65] M. Krüger, F. Weysser, and T. Voigtmann, Phys. Rev. E **81**, 061506 (2010).
- [66] W. Feller, *An Introduction to Probability Theory and Its Applications*, 2nd ed., Vol. II (Wiley & Sons, New York, 1971).
- [67] R. A. Usmani, Lin. Alg. Appl. **212/213**, 413 (1994).
- [68] C. H. Ziener, M. Rückl, T. Kampf, W. R. Bauer, and H. P. Schlemmer, J. Comput. Appl. Math. **236**, 4513 (2012).